AGU PUBLICATIONS

Geophysical Research Letters

RESEARCH LETTER
10.1002/2015GL063628

Key Points:
- Linear relation found between wave attenuation and pancake ice thickness
- Linear relation found between eddy viscosity and ice thickness in viscous model
- Simple expression derived to calculate attenuation at any period

Correspondence to:
M. J. Doble,
doble@obs-vlfr.fr

Citation:
Doble, M. J., G. De Carolis, M. H. Meylan, J.-R. Bidlot, and P. Wadhams (2015), Relating wave attenuation to pancake ice thickness, using field measurements and model results, *Geophys. Res. Lett.*, *42*, doi:10.1002/2015GL063628.

Received 25 FEB 2015
Accepted 12 MAY 2015
Accepted article online 14 MAY 2015

Relating wave attenuation to pancake ice thickness, using field measurements and model results

Martin J. Doble[1], Giacomo De Carolis[2], Michael H. Meylan[3], Jean-Raymond Bidlot[4], and Peter Wadhams[5]

[1]Observatoire Océanologique, UPMC Univ Paris 06, UMR 7093, LOV, Villefranche-sur-mer, France, [2]CNR-IREA, Milan, Italy, [3]School of Mathematical and Physical Science, University of Newcastle, Callaghan, New South Wales, Australia, [4]European Centre for Medium-Range Weather Forecasting, Reading, UK, [5]Department of Applied Maths and Theoretical Physics, University of Cambridge, Cambridge, UK

Abstract Wave attenuation coefficients (α, m^{-1}) were calculated from in situ data transmitted by custom wave buoys deployed into the advancing pancake ice region of the Weddell Sea. Data cover a 12 day period as the buoy array was first compressed and then dilated under the influence of a passing low-pressure system. Attenuation was found to vary over more than 2 orders of magnitude and to be far higher than that observed in broken-floe marginal ice zones. A clear linear relation between α and ice thickness was demonstrated, using ice thickness from a novel dynamic/thermodynamic model. A simple expression for α in terms of wave period and ice thickness was derived, for application in research and operational models. The variation of α was further investigated with a two-layer viscous model, and a linear relation was found between eddy viscosity in the sub-ice boundary layer and ice thickness.

1. Introduction

The yearly advance and retreat of the Antarctic sea ice cover is one of the largest seasonal changes on the planet, yet the initial phase of ice formation, in the form of pancake and frazil ice, has received relatively little attention compared to congelation (pack) ice. Earlier papers have attempted to quantify the growth processes and the elevated growth rate of the pancake ice cover relative to that which would be expected from a congelation ice cover [*Doble et al.*, 2003; *Doble*, 2009], as well as the dynamics of the pancakes, again contrasted with pack ice [*Doble and Wadhams*, 2006].

The factor which controls the transition of the ice cover from pancake to pack ice is the presence of waves, usually traveling into the ice from the open ocean. The attenuation of these waves with distance is the main factor in determining the extent of the pancake zone, and thus the total area over which elevated ice production rates occur. If we are to understand and model the evolution of the Antarctic ice cover, we must therefore quantify this loss of wave energy.

The history of field measurements of waves in pancake ice is rather short, since the harsh wave-influenced environment is particularly destructive to floating measuring devices. The deployment of a six-buoy array from the Alfred Wegener Institute vessel *Polarstern* in April 2000 represents almost the only field wave measurement in pancake ice to date. These measurements are analyzed in the current study. Additional waves-in-pancakes data come from laboratory tank tests, beginning with *Newyear and Martin* [1999] and continuing recently [*Wang and Shen*, 2010] as interest in the role of waves in the Arctic has grown.

Other techniques have used satellite synthetic aperture radar (SAR) images to extract directional wave spectra in the pancake/frazil zone, using inversion techniques. The change in wave dispersion as the waves enter the ice can be used to infer the ice thickness. First attempts used a mass-loading model and gave ice thicknesses that were far too high [*Wadhams et al.*, 1999, 2002; *Wadhams and Holt*, 1991]. The wave propagation model in pancake ice was then changed to that of *Keller* [1998], in which the pancake/frazil ice is represented by a highly viscous fluid, lying on top of an inviscid ocean [*Wadhams et al.*, 2004]. The unknown parameter in the model is the viscosity of the pancake/frazil mix. Fitting results to the mean pancake ice thickness data measured from the same *Polarstern* cruise (24 cm) gave an ice cover viscosity of $5\times10^{-2}\,m^2\,s^{-1}$, agreeing with laboratory-scale measurements [*Newyear and Martin*, 1999] and suggesting that similar physics applies at these very different scales.

The focus of the current paper is relating wave attenuation to the thickness of the pancake/frazil ice cover that the waves traverse. The aim is to derive an expression for wave attenuation coefficient, α (m^{-1}), in terms of wave period and ice properties, which can then be easily applied to wave-in-ice models, research, or operational. We also seek to understand the results in terms of a two-layer viscous model, again searching for an easily computed relation to derive the unknown parameters to constrain the model, in order that these can find ready application.

The aim of the paper is not model validation, since the series of two-point measurements discussed here is insufficient for that task. The aim is to take the standard models and use them to develop relations between attenuation and ice properties, assuming they apply.

We first describe the buoy deployment, the instruments, and the models used. Buoy wave data are then presented for a 12 day period from deployment until the pancake ice surrounding the outermost buoys in the array consolidated into solid pack ice. Time and frequency varying attenuation coefficients are then calculated and a novel relation with ice thickness derived. Attenuation coefficients are then compared with published data in the "classic," broken floe, Arctic and Antarctic marginal ice zones (MIZs). Finally, results are simulated using a common two-layer viscous model, whose controlling parameters are also related to ice thickness for the first time.

2. Methods

2.1. Deployments

An array of custom-built buoys was deployed into the advancing marginal ice zone of the Weddell Sea between 17 and 20 April 2000, from the icebreaker *Polarstern*. The buoys were deployed in a "five dice" pattern; with one buoy at each corner of a ~100 km square and the fifth unit in the center. Outer buoys were deployed in new pancakes, approximately 70 cm in diameter and 5–10 cm thick, at 50–60% concentration with frazil ice filling the interstices. Inner buoys were deployed at the limit of the pancake zone, 10–15 km seaward of the northernmost consolidated pack ice. Detailed conditions have been reported in previous papers [*Doble et al*., 2003; *Wadhams et al*., 2004].

2.2. Instruments

Each buoy contained a vertical accelerometer (Crossbow CXL02LF1Z), mounted at the center of buoyancy and sampled at 2 Hz for approximately 26 min every 3 h. Onboard processing transformed the acceleration data to vertical displacement (double integration) and calculated the one-dimensional wave spectrum at 56 frequencies. A "Welch" scheme was used to give the smallest possible variance per data point [*Welch*, 1967] and is broadly equivalent to that used in the industry standard Waverider buoy. Recent measurements [*Kohout et al*., 2014] used an identical scheme, based on our source code. Spectra were transmitted over the low-Earth orbit *Orbcomm* satellite system, this being before the availability of *Iridium* communications.

2.3. Wave Model

Since the buoys only measured the vertical wave spectrum, the incoming wave propagation direction was determined using the European Centre for Medium-Range Weather Forecasts wave model (WAM). Using the outer buoy as a starting point, the nearest points on the WAM grid (1° latitude and longitude) were examined, taking account of the travel time of the waves to reach the buoys. The closest grid point having a wave propagation direction which intercepted the buoy within a tolerance of ±15° was selected as the "wave origin." Comparison between buoy and model data when buoys were close to the ice edge [*Doble and Bidlot*, 2013] showed that the WAM results closely matched the buoy spectra, giving confidence in the directions used here.

2.4. Two-Layer Viscous Model

Pancake ice—having small element sizes compared to the wavelengths traveling through them—can be represented as a viscous fluid layer. Ice viscosity accounts for the energy-consuming interactions of the incident wave energy which may occur within the ice layer, such as bending, deformation of the ice slurry, and collisions between pancakes. The underlying ocean is also assumed viscous. Here the viscosity is not the molecular viscosity but describes the turbulent eddies which develop beneath the ice layer. In this

context, the concept of eddy viscosity coefficient can be used to parameterize the turbulent water flow in the ice water boundary layer.

The two-layer viscous model used in this study considers the ice cover (upper layer) and the underlying ocean (lower layer) as Newtonian incompressible fluids, each with its own thickness h, kinematic viscosity ν, and density ρ. The ice layer is considered more viscous than the underlying ocean, and ice density is a function of ice composition and concentration. The fluid motion is described by the laminar Navier-Stokes equations with boundary conditions specified at the air/ice, ice/water interfaces, and at the rigid seabed. Assuming spatial wave energy decay, the relation dispersion is obtained in implicit form, thus requiring a numerical inversion procedure to obtain the in-ice values of spatial attenuation rate and wave number of the incident wave as a function of the incident wave period. The mathematical details can be found in *De Carolis and Desiderio* [2002].

3. Results

A progressive reduction in significant wave height was observed through the buoy array, with the outer buoy experiencing up to 3.7 m waves and the middle buoy up to 1.1 m. The inner buoy did not measure significant wave activity. Mean periods tell a similar story, with the outer buoy measuring periods as low as 5 s, the middle buoy experiencing 8 s minimum, and the inner buoy displaying long mean periods throughout. We thus limit the current analysis to the two buoys which experienced significant waves.

3.1. Attenuation Measurements Between Buoys

We calculate attenuation using the standard equation below

$$E_f(x) = E_f(0).\exp(-ax), \tag{1}$$

where α is the frequency-dependent attenuation coefficient, E_f (x) is the energy density (m^2 s) at center frequency f and penetration x. This parameterization only assumes that the decay is linear—i.e., independent of wave amplitude—and can thus be separated into frequency components, each of which decays proportionally to amplitude. These assumptions are supported by the data. More broadly, the assumption of viscous behavior (i.e., ice elements very much smaller than the wavelength) precludes floe bending and constrains earlier general expressions for decay [*Wadhams*, 1973] to a flow law regime of $n = 1$, again pointing to an exponential decay. We thus proceed with this assumption.

The calculated spectral attenuation coefficient is shown in Figure 1, for 95 instances during the period of interest. Color contours show $\log_{10}(\alpha)$, varying in both time (x axis) and with period (y axis). The plot displays two major characteristics: (1) increasing attenuation at short periods; and (2) highly variable attenuation at all frequencies, with, for example, attenuation at the dominant period of 8 s varying over at least 2 orders of magnitude.

The path length between measurements can be calculated in several ways, introducing further variation due to the changing geometry of wave directions, buoy positions, and the ice conditions. Attenuation was calculated using three distances (1) the direct buoy-to-buoy distance, (2) the distance between buoys along the dominant wave direction, or (3) the difference in penetration between the buoys perpendicular to an assumed-linear ice edge. Variation in the distances calculated by these methods was in fact relatively small, and the form of the variability (which interests us most) was preserved in all cases. We thus present results using only "distance along the dominant wave direction" here. Change in wave direction on entering the ice (refraction) is ignored, as it is negligible compared with distortions due to factors such as ice edge geometry and ice inhomogeneity.

In the first half of the record, the array underwent significant compression as it came under the influence of northerly (on-ice) winds from an approaching depression. The two buoys were initially separated by 43 km, but this reduced to only 8 km before southerly winds drove the ice edge north once again. The changing characteristics of the ice cover during this period are likely to have a significant effect on the wave attenuation. Accordingly, we track the ice thickness using the process model detailed by *Doble* [2009], which takes into account mechanical redistribution of ice thickness, thermodynamic ice growth/melt, and the transition from frazil ice to pancakes. "Ice thickness" in this context is the equivalent solid ice thickness, using the ice volume fractions in pancakes (0.7) and frazil ice (0.4) measured in situ during deployment of the buoys [*Doble et al.*, 2003] by bringing pancakes on board ship and examining the frazil in a clear

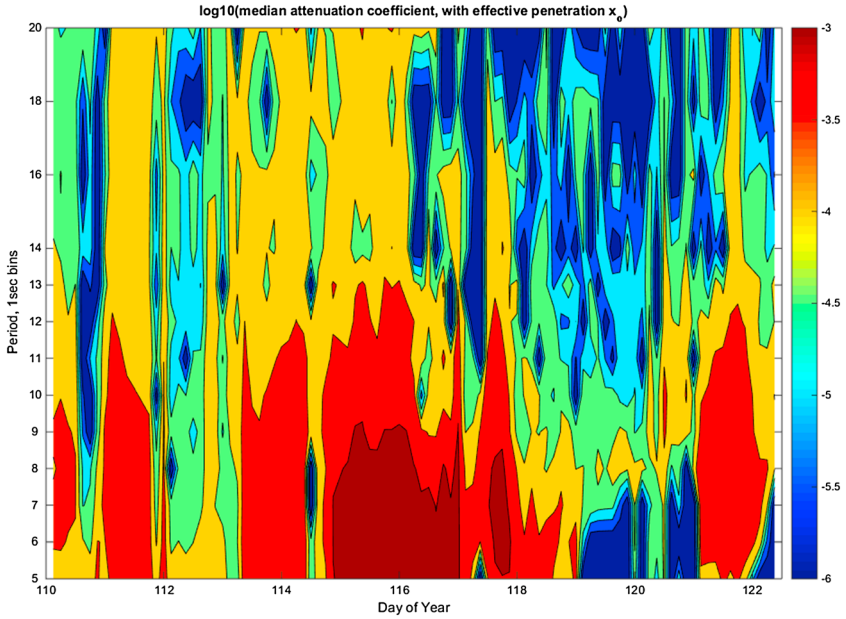

Figure 1. Variation of the calculated attenuation coefficient between two buoys—log10(α), colors—plotted with time (x axis) and period (y axis).

sampling tube. Area fraction of the two ice types was measured during buoy deployment with aerial photography transects from the ship's helicopters and subsequently tracked by the model. Direct (e.g., satellite) observation of ice concentration would only be possible with high-resolution synthetic aperture radar (SAR) imagery, which was not acquired. Equivalent solid ice thickness within the array changes from 5 cm at the beginning of the period to nearly 55 cm at the end. The frazil and pancake mixture can be represented by a single number, since both ice types—and the horizontal scale of variation between them—are small compared with the wavelengths considered.

Examining the variation of attenuation coefficient against modeled ice thickness (Figure 2, plotted for 8 s period, near the peak of the energy spectrum) initially shows rather scattered points. However, if data from the compression phase (blue circles, prior to day 116) are separated from the subsequent reexpansion (red crosses, day 116 onward), a clear linear relation between ice thickness and attenuation coefficient exists during the compression phase.

The expansion case is less defined, and on a significantly different gradient. We attribute this deviation to very heterogeneous ice thickness during expansion, when the rafted pancake ice would diverge in a "clumpy" manner. While pancakes will raft under compression to smoothly increase ice thickness, the reverse is not true. Thus, the diverged ice cover will likely consist of alternating bands of ice and open water. The expansion phase is also marked by a significant rotation of the array, meaning the two buoys are no longer aligned with the waves, further complicating the geometry. Finally, as the wind has reversed direction, the sea may become confused and thus mathematically challenging.

A similar linear relation during compression is displayed for all wave periods present in the data, with the linear fit having a decreasing gradient with increasing period: longer waves are less sensitive to ice thickness, as expected. The linear fits are constrained to pass through the origin to derive a gradient (p) at each period. This gradient itself varies linearly with wave period between 7 and 14 s period, as shown by the inset in Figure 2. There is very little energy above 14 s, thus attenuation cannot be represented by these data. Below 7 s, we see the classic "rollover" in attenuation, seen in all previous measurements [*Wadhams et al.*, 1988]. We attribute this to the fact that energy at such short periods from the open ocean has already been attenuated before it reaches the outermost buoy. Equation (2) allows the calculation of α if ice thickness (h_{eq}) and T are known

$$a = (pT + C)\,.\,h_{eq}, \tag{2}$$

where $p = -4.2 \times 10^{-4}$ and $C = 6.2 \times 10^{-3}$

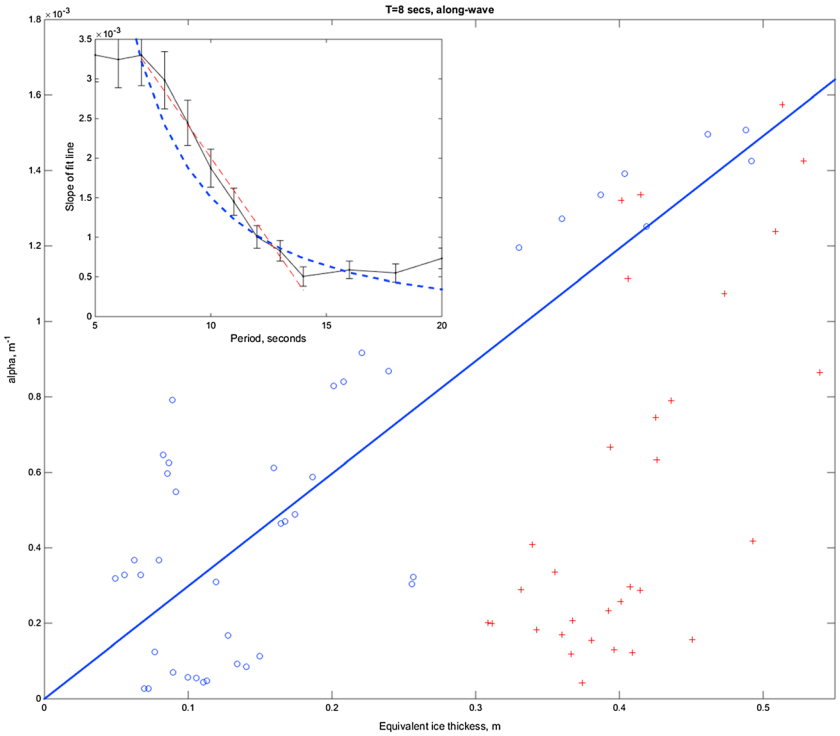

Figure 2. The main figure shows the calculated attenuation coefficient (α) plotted against modeled ice thickness, for 8 s period. Blue dots are during the compressive phase of array dynamics, red dots during dilation. The gradient of the blue fit line (constrained to pass through the origin) is plotted for all periods in the inset figure (black line, with error bars). The red fit line gives the relation expressed in equation (1). The blue curve shows a squared (power law) fit to the same data.

As shown in the inset for Figure 2, the form of the fitted gradients also suggests an inverse squared relation with period (blue curve), which is more intuitive, given the viscous nature of the ice. The power law also has the advantage of not being limited to the smaller range of periods required for the linear fit. The fitted power law shown in the figure is given by

$$a = 0.2T^{-2.13}h_{\mathrm{eq}}. \tag{3}$$

Figure 3 (left) presents a contour plot of the measured α/T relation, with pancake/frazil equivalent ice thickness (m) as the color contours. Clearly, high equivalent ice thickness (red colors) maps to high attenuation coefficients at all periods, and vice versa. Figure 3 (right) shows the equivalent result for equation (3) fit. For practical purposes, only the attenuation in the periods of significant wave energy is important for large-scale wave models and for these models either of our simple parametrizations (linear or power law) is applicable.

We find no relation between attenuation coefficient and wave amplitude, which implies that the process is linear as was found in *Meylan et al*. [2014], validating our earlier assumption ex post.

3.2. Two-Layer Viscous Model Predictions

Comparison of wave attenuation with the two-layer viscous model was carried out in the range of wave periods which showed a consistent trend of increasing attenuations for decreasing wave periods.

The two-layer viscous model was inverted to estimate eddy viscosity and ice viscosity parameters under a deep water assumption. The constrained Levenberg-Marquardt least squares fit was used [*Moré*, 1978; *Markwardt*, 2009]. Ice thicknesses were assumed known and equal to the equivalent solid ice thickness. Averaging over frequency intervals was done to increase the data's degrees of freedom (DOF) to 81 ($f < 0.1$ Hz) and 135 ($f >= 0.1$ Hz). The data can thus be assumed to be Gaussian distributed with 1σ overall uncertainty being a function of the wave frequency, expressed as $\sigma = \beta/D_{\mathrm{w}}$, where D_{w} is the distance separating buoys along the dominant wave direction. Values of σ varied between 0.6×10^{-5} and 31×10^{-5}.

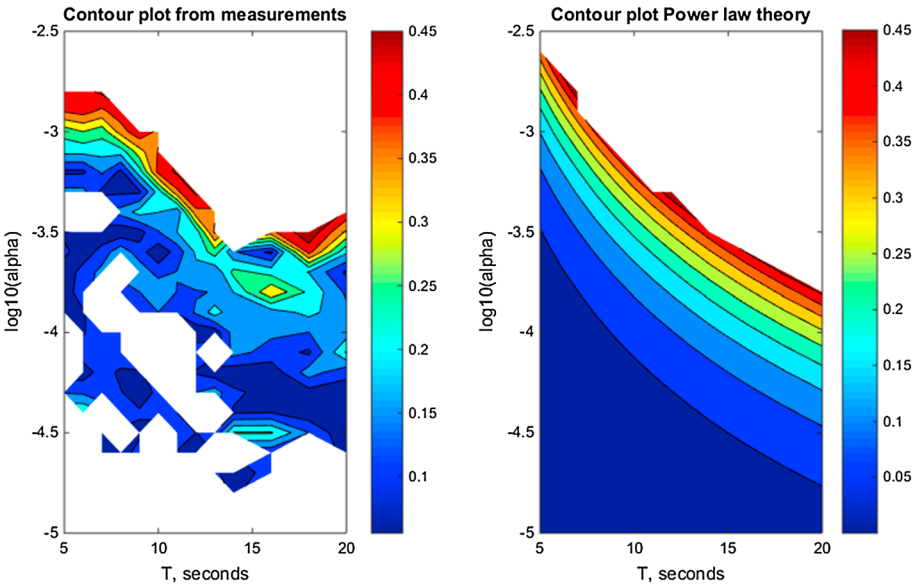

Figure 3. A contour plot showing ice thickness (colors, meters) variation with changing period (x axis) and attenuation coefficient (α). (left) The measured results: thicker ice plots to higher alphas at all periods. (right) The fitted square law (equation (3)) equivalent.

A total of 84 instances were available for this analysis. Fits were reliable with acceptably low χ^2 values for 72 instances.

Inversion results showed two regimes of wave attenuations. The first is well described by constant ice viscosity and variable eddy viscosity. The most appropriate ice viscosity value was approximately 0.01 $m^2 s^{-1}$—consistent with previously reported values on grease ice grown in laboratory [*Newyear and Martin*, 1999] and pancake ice [*Wadhams et al.*, 2004]. This correspondence with laboratory results is not assumed or required in our analysis. Attenuation rates are thus dependent on the ice thickness h and the eddy viscosity ν_e. Eddy viscosity was well correlated with ice thicknesses, as shown in Figure 4. The linear best fit between $\ln\nu_e$ and ice thickness is shown on the plot as continuous line

$$\ln\nu_e = -5.36 + 6.88\ h, \quad r^2 = 0.92. \tag{4}$$

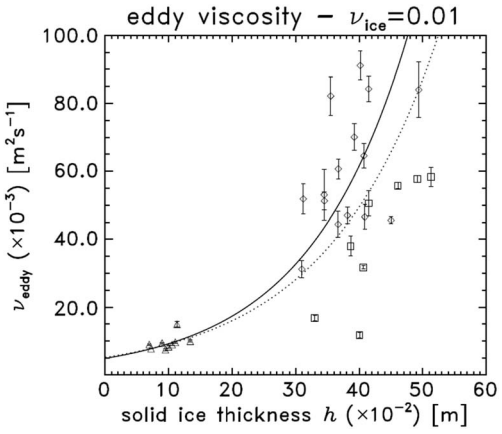

Figure 4. Retrieved eddy viscosity as a function of the solid ice thickness corresponding to $\nu_{ice} = 0.01\ m^2 s^{-1}$ obtained assuming the ice cover as viscous layer (triangle and diamond points) and viscoelastic layer (square points). Triangle points are relevant to instances collected on days before 116; diamond points are relevant to those on days after 116; square points are relevant to the viscoelastic cases described in main body text that occurred on days 115 and 116.

In contrast, a second attenuation regime is characterized by widely varying values of ice viscosity, ν_{ice}, in the range 0.1–6920 $m^2 s^{-1}$ with an average over all instances of 765 $m^2 s^{-1}$. Eddy viscosity values are no longer correlated with ice thickness. To explain such high values of pancake ice viscosity, we considered the role of ice layer elasticity in affecting wave propagation. Elasticity may come from either the pancakes themselves (unlikely, given the small element size compared to the wavelength) or the composite ice sheets as a whole. According to the Voigt viscoelastic continuum model [*Wang and Shen*, 2010], both ice viscosity and elasticity can be represented with a complex-valued ice layer viscosity defined as follows:

$$\nu_1 = \nu_{ice} + iG/\omega\rho_{ice}, \tag{5}$$

where G is the shear modulus of pancake ice and $\omega = 2\pi f$.

Inversion runs were performed assuming that $G = 2 \times 10^9$ Pa is a realistic value for young sea ice [*Anderson*, 1958], hence also representative for pancake ice. Significantly improved results were obtained for instances collected on days 115, 116, and on the beginning of day 117, i.e., at the end of the array compressive phase when pancake ice had presumably reached its highest state of rafting and solidity. For this time interval, the inverted values of ice viscosity decreased, from a value of 437 (for the pure viscous model) to 58 $m^2 s^{-1}$ (for the viscoelastic model). In eight cases, a value of 0.01 was retrieved. The corresponding eddy viscosity values are well correlated with those obtained using the pure viscous model (see Figure 4). Together, the linear best fit between eddy viscosity and ice thickness is plotted as a dotted line

$$\ln \nu_e = -5.26 + 5.64 \ \mathrm{h}, \quad r^2 = 0.76. \tag{6}$$

4. Discussion and Conclusions

Most importantly, we have demonstrated a clear linear relation between pancake ice thickness and spectral wave attenuation for the first time, and derived a simple expression for α in terms of the wave period and ice thickness. Linking the two parameters using ice thickness output by the *Doble* [2009] model allows us to finally understand the highly variable field data, which hitherto has prevented its meaningful analysis. Values of the attenuation coefficient seen are up to 2 orders of magnitude greater than previous measurements in the "broken floe MIZ," in both Arctic and Antarctic, as reported in *Wadhams et al*. [1988] and *Kohout et al*. [2014]. This is perhaps counterintuitive, given the greater ice thicknesses (up to 4.0 m) present in those more "classic" MIZs, though the dominant energy dissipation mechanism there—currently presumed to be scattering—is of a completely different nature to the viscous eddy dissipation which takes place in the pancake fields.

We would not expect the demonstrated linear relation to hold in the scattering regime, since the horizontal floe size (and hence the number of floes edges in a given path length) is the dominant factor there (a squared relation), despite the scattering term also having a linear ice thickness relation, as already known [*Wadhams*, 1975].

A linear relation between modeled (log) eddy viscosity and pancake/frazil ice thickness has also been newly demonstrated using these data, with fitted eddy viscosities at the ice water boundary ranging from 0.01 $m^2 s^{-1}$ ($h = 10$ cm) to 0.2 $m^2 s^{-1}$ ($h_i = 50$ cm). These values are encouraging: available field measurements of eddy viscosity under large-ice floes report the value of 0.24×10^{-2} m^2/s in the central Arctic Ocean [*Hunkins*, 1966]; in the Antarctic MIZ, Weddell Sea, slightly larger values were reported ranging from 1.6×10^{-2} m^2/s [*Brennecke*, 1921] to 2.0×10^{-2} m^2/s [*McPhee and Martinson*, 1994]. Since the variability of eddy viscosity reflects the actual turbulence level at the measurement site, the higher values found in the present study are expected, since the turbulence levels during our measurements (e.g., $H_s = 3.7$ m) are considerably higher than for the quoted cases. Turbulence levels are nevertheless low enough that the assumed laminar motion of the model is not violated. The linear approach we have adopted thus appears valid. Clearly, there will be nonlinear effects, but for the amplitudes and periods present in these field data, the linear effects are dominant.

In this context, it might be expected that eddy viscosity would negatively correlate with ice thickness, since the wave height between buoys drops through the record. We suggest that the increased underside roughness of the rafted pancakes as they compact (cf. the rather smooth underside of individual pancakes) dominates the evolution of eddy viscosity in this time series.

It should be borne in mind that this application of the viscous model is not a validation, which would require more extensive data than so far available. We merely state that if the model applies, then its controlling parameter (eddy viscosity) can be related simply to ice thickness. The viscous results also give insight into the changing properties of the ice cover as the loose pancake/frazil mix is compressed against the pack ice toward day 116. It appears that the ice cover begins to take on elastic properties as the individual pancakes raft and begin to form a more contiguous sheet.

For the elastic regime, we accept that the constant value of shear modulus is likely unrepresentative. The rafted pancakes would have remained unconsolidated until day 116—in the warm air temperatures (−2°C) during the on-ice winds—and only frozen together once winds turned southerly and temperatures

plummeted to −15°C and below [see Figure 5, *Doble et al*., 2003]. The purpose of the elastic term is primarily to give insight into the two-layer model, which does not parameterize the complex changes undergone by the ice cover described. Retrieved ice viscosities are therefore forced spuriously high, in an ice cover that can no longer be described as viscous.

It is worth pointing out that, even in the reliably stormy, on-ice wind and wave conditions of the Antarctic MIZ, the ideal geometry—a large-scale linear ice edge with waves impinging perpendicularly upon it and traveling through an ice cover which is homogenous for tens of kilometers—is hard to find. Real-world experimental setups immediately require us to make assumptions about the path length, x, over which the attenuation is measured, as discussed in the previous section. This inevitably increases scatter in calculated attenuation coefficients. Pancake fields at least do not require assumptions about the directional spreading or collimation of the waves in ice—currently under investigation for broken-floe MIZs—since the small elements allow passage of the waves with little deviation and spreading. This can observed during helicopter flights over the pancake ice regions [e.g., *Doble*, 2008].

As mentioned in section 1, the aim of the study was to provide computationally simple parameterizations for wave attenuation in pancake/frazil ice. Equations in ice thickness and wave period can now be used in research and operational models to determine the extent of the wave-influenced pancake zone, though further measurements to verify the wider applicability of this data set are required.

Systematic SAR observations from available satellite platforms can provide such measurements. Combining the new expression for α as a function of the wave period and ice thickness with the predictions of the two-layer viscous model, an inversion procedure of the SAR image spectra can be envisaged to estimate the ice thickness over fields of pancakes in the MIZ at unprecedented spatial resolution.

Such vast fields of pancake ice have traditionally only been associated with the advancing Antarctic MIZ, and, on a smaller scale, the Greenland Sea Odden—though that last formed in 2007. The increased open water area present in the autumn Arctic Ocean, particularly in the Beaufort Sea [*Lee et al*., 2012; *Jeffries et al*., 2013], will make it increasingly applicable to those seas as well, and these findings are thus particularly timely.

Acknowledgments

The field experiment was carried out as part of the "Short Timescale Motion of Pancake Ice" (STiMPI) project, funded by the UK Natural Environment Research Council (grant GR3/12952) and supported by the Alfred Wegener Institute vessel *F/S Polarstern*. M.J.D. and P.W. were funded during this analysis by the Office of Naval Research "Sea State" Departmental Research Initiative (grant N00014-13-1-0290); G.D.C. was funded by the MIUR-PNRA, PANACEA project (grant 2013/AN2.02) and FP7 EU project ICE-ARC (grant agreement 603887). The data discussed in the paper can be obtained by contacting the lead author.

The Editor thanks an anonymous reviewer for assisting in the evaluation of this paper.

References

Anderson, D. L. (1958), Preliminary results and review of sea ice elasticity and related studies, *Trans. Eng. Inst. Can.*, *2*, 116–122.

Brennecke, W. (1921), Die ozeanographischen Arbeiten der Deutschen Antarktischen Expedition 1911–1912, *Arch. Dtsch. Seewarte*, *39*, 1–216.

De Carolis, G., and D. Desiderio (2002), Dispersion and attenuation of gravity waves in ice: A two-layer viscous fluid model with experimental data validation, *Phys. Lett. A*, *305*, 399–412.

Doble, M. J. (2008), Growth and motion at the Weddell Sea ice edge, PhD thesis, Univ. of Southampton, 168 pp.

Doble, M. J. (2009), Simulating pancake and frazil ice growth in the Weddell Sea: A process model from freezing to consolidation, *J. Geophys. Res.*, *114*, C09003, doi:10.1029/2008JC004935.

Doble, M. J., and J.-R. Bidlot (2013), Wavebuoy measurements at the Antarctic sea ice edge compared with an enhanced ECMWF WAM: Towards global waves-in-ice modelling, *Ocean Modell.*, *70*, 166–173, doi:10.1016/j.ocemod.2013.05.012.

Doble, M. J., and P. Wadhams (2006), Dynamical contrasts between pancake and pack ice, investigated with a drifting buoy array, *J. Geophys. Res.*, *111*, C11S24, doi:10.1029/2005JC003320.

Doble, M. J., Coon, M. D., and P. Wadhams (2003), Pancake ice formation in the Weddell Sea, *J. Geophys. Res.*, *108*(C7), 3209, doi:10.1029/2002JC001373.

Hunkins, K. (1966), Ekman drift currents in the Arctic Ocean, *Deep Sea Res.*, *13*(4), 607–620, doi:10.1016/0011-7471(66)90592-4.

Jeffries, M. O., J. E. Overland, and D. K. Perovich (2013), The Arctic shifts to a new normal, *Phys. Today*, *66*, 35–40.

Keller, J. B. (1998), Gravity waves on ice-covered water, *J. Geophys. Res.*, *103*(C4), 7663–7669, doi:10.1029/97JC02966.

Kohout, A. L., M. J. M. Williams, S. Dean, and M. H. Meylan (2014), Storm-induced sea ice breakup and the implications for ice extent, *Nature*, *509*, 604–607, doi:10.1038/nature13262.

Lee, C. M., et al. (2012), Marginal Ice Zone (MIZ) program: Science and experiment plan, *Tech. Rep., APL-UW 12–01,* Applied Physics Lab., Univ. of Washington.

Markwardt, C. B. (2009), Non-linear least squares fitting in IDL with MPFIT, in *Proc. Astronomical Data Analysis Software and Systems XVIII*, Que., Can., ASP Conf. Ser., vol. 411, edited by D. Bohlender, P. Dowler, and D. Durand, pp. 251–254, Astronomical Society of the Pacific, San Francisco, Calif.

McPhee, M. G., and D. G. Martinson (1994), Turbulent mixing under drifting pack ice in the Weddell Sea, *Science*, *263*(5144), 218–221, doi:10.1126/science.263.5144.218.

Meylan, M. H., L. G. Bennetts, and A. L. Kohout (2014), In situ measurements and analysis of ocean waves in the Antarctic marginal ice zone, *Geophys. Res. Lett.*, *41*, 5046–5051, doi:10.1002/2014GL060809.

Moré, J. (1978), The Levenberg-Marquardt algorithm: Implementation and theory, in *Numerical Analysis*, vol. 630, edited by G. A. Watson, p. 105, Springer, Berlin, doi:10.1007/BFb0067690.

Newyear, K., and S. Martin (1999), Comparison of laboratory data with a viscous two-layer model of wave propagation in grease ice, *J. Geophys. Res.*, *104*(C4), 7837–7849, doi:10.1029/1999JC900002.

Wadhams, P. (1973), Attenuation of swell by sea ice, *J. Geophys. Res.*, *78*(18), 3552–3563, doi:10.1029/JC078i018p03552.

Wadhams, P. (1975), Airborne laser profiling of swell in an open ice field, *J. Geophys. Res.*, *80*(33), 4520–4528, doi:10.1029/JC080i033p04520.
Wadhams, P., and B. Holt (1991), Waves in frazil and pancake ice and their detection in Seasat synthetic aperture radar imagery, *J. Geophys. Res.*, *96*(C5), 8835–8852, doi:10.1029/91JC00457.
Wadhams, P., V. A. Squire, D. J. Goodman, A. M. Cowan, and S. C. Moore (1988), The attenuation rates of ocean waves in the marginal ice zone, *J. Geophys. Res.*, *93*(C6), 6799–6818, doi:10.1029/JC093iC06p06799.
Wadhams, P., F. E. Parmiggiani, G. de Carolis, and M. Tadross (1999), Mapping the thickness of pancake ice using ocean wave dispersion in SAR imagery, in *The Oceanography of the Ross Sea, Antarctica*, edited by G. Spezie and G. M. R. Manzella, pp. 17–34, Springer, Milan.
Wadhams, P., F. E. Parmiggiani, and G. de Carolis (2002), The use of SAR to measure ocean wave dispersion in frazil–pancake ice fields, *J. Phys. Oceanogr.*, *32*(6), 1721–1746.
Wadhams, P., F. F. Parmiggiani, G. De Carolis, D. Desiderio, and M. J. Doble (2004), SAR imaging of wave dispersion in Antarctic pancake ice and its use in measuring ice thickness, *Geophys. Res. Lett.*, *31*, L15305, doi:10.1029/2004GL020340.
Wang, R., and H. Shen (2010), Gravity waves propagating into an ice-covered ocean: A viscoelastic model, *J. Geophys. Res.*, *115*, C06024, doi:10.1029/2009JC005591.
Welch, P. D. (1967), The use of fast Fourier transform for the estimation of power spectra: A method based on time averaging over short, modified periodograms, *IEEE Trans. Audio Electroacoust.*, *AU-15*, 70–73.